

Microscopic theory of the Coulomb based exchange coupling in magnetic tunnel junctions

O. G. Udalov

Department of Physics and Astronomy, California State University Northridge,
Northridge, CA 91330, USA

Institute for Physics of Microstructures, Russian Academy of Science, Nizhny
Novgorod, 603950, Russia

E-mail: oleg.udalov@csun.edu

I. S. Beloborodov

Department of Physics and Astronomy, California State University Northridge,
Northridge, CA 91330, USA

PACS numbers: 75.50.Tt 75.75.Lf 75.30.Et 75.75.-c

Abstract. We study interlayer exchange coupling based on the many-body Coulomb interaction between conduction electrons in magnetic tunnel junction. This mechanism complements the known interaction between magnetic layers based on virtual electron hopping (or spin currents). We find that these two mechanisms have different behavior on system parameters. The Coulomb based coupling may exceed the hopping based exchange. We show that the Coulomb based exchange interaction, in contrast to the hopping based coupling, depends strongly on the dielectric constant of the insulating layer. The dependence of the interlayer exchange interaction on the dielectric properties of the insulating layer in magnetic tunnel junction is similar to magneto-electric effect where electric and magnetic degrees of freedom are coupled. We calculate the interlayer coupling as a function of temperature and electric field for magnetic tunnel junction with ferroelectric layer and show that the exchange interaction between magnetic leads has a sharp decrease in the vicinity of the ferroelectric phase transition and varies strongly with external electric field.

Submitted to: *J. Phys.: Condens. Matter*

magneto-electric effect, multiferroics, Coulomb interaction, magnetic tunnel junction, exchange interaction:

1. Introduction

Magnetic tunnel junctions (MTJ) are of great importance these days because of their promise for next generation memory cells [1, 2, 3, 4, 5, 6]. However, there are several issues to create such memory cells. One of them is control of magnetic state of ferromagnetic (FM) leads in MTJ. This problem requires a fundamental research and understanding of spin currents and interlayer exchange coupling (IEC) mechanisms in MTJ. The IEC was studied theoretically [7, 8, 9, 10, 11, 12, 13, 14, 15] and experimentally [16, 17, 12, 16, 18, 19, 20, 21, 22] in numerous papers. These works show that there are several phenomena responsible for magnetic coupling between FM layers in MTJ. A weak FM coupling appears due to magneto-dipole (MD) interaction between correlated roughness in MTJ interfaces (orange peel effect) [23, 24]. Spin currents across the insulating barrier in MTJ produce the hopping based exchange interaction [7, 8, 9] leading to the FM or antiferromagnetic (AFM) coupling depending on the system parameters [17, 18]. In addition, the IEC was studied for insulating layer with impurities [10, 25, 12]. This mechanism gives the AFM contribution to the total magnetic coupling between FM leads. In this paper we propose a different mechanism of IEC in MTJ based on many-body Coulomb interaction.

The hopping based IEC in MTJ was studied both analytically [7, 8, 9, 10, 13, 15] and using the *ab initio* calculations [11, 12, 14]. To derive the IEC the single particle Hamiltonian was used with kinetic term and the spin-dependent single-particle potential. The many-body interaction was not taken into account when calculating the IEC.

The exchange coupling exists due to many-particle effects, for example due to the Coulomb interaction. The indirect Coulomb interaction (exchange) between electrons localized at different atoms is responsible for FM and AFM states in magnetic insulators [26]. The indirect Coulomb interaction between conduction and localized electrons in FM metals results in spin subband splitting of the conduction band [26]. In this paper we study the IEC based on the inter-electron Coulomb interaction between two FM metallic leads separated by the insulating layer.

The basic idea behind this mechanism is related to the fact that the wave functions of electrons located at different FM leads are overlapped inside the insulating layer. Since the screening effects inside the insulator are weak the long-range Coulomb interaction between these electrons exists and it has the spin-dependent part (exchange interaction) [27]. Here we study the IEC due to this indirect spin-dependent part of the Coulomb interaction and show that this contribution is comparable and even bigger than the hopping based exchange coupling.

The most important feature of the Coulomb based exchange interaction is its dependence on the dielectric permittivity of the insulating layer. This dependence can be used to distinguish this contribution from other contributions to the exchange coupling. Also this peculiarity allows to realize the magneto-electric (ME) coupling [28, 29] in MTJ with ferroelectric (FE) insulating barrier. Generally, ME effects in MTJ are known even without the FE barrier. Applying voltage to the MTJ leads to the deformation of the

barrier potential profile and to variation of hopping based IEC [30, 31, 32, 33]. Spin transfer torque effect also appear in the voltage biased MTJ leading to magnetization dynamics [8, 34, 35, 30, 31, 32, 33]. The ME effect in MTJ with FE barrier was studied in several works [10]. The FE creates the surface charges at the interfaces between the barrier and FM leads. These charges modify the potential barrier profile and influence the IEC. Switching FE polarization with electric field allows to change the magnitude of IEC. All mentioned effects are related to the hopping based IEC. In the current manuscript we propose a completely different mechanism based on many-body effects.

The paper is organized as follows. In section 2 we introduce the model for MTJ. In sections 4 and 5 we calculate the inter-electron Coulomb interaction and the IEC in the system. We discuss and compare the Coulomb and the hopping based IEC in section. 6. We consider ME coupling in MTJ with FE barrier in section 6. Finally, we discuss validity of our theory in section 7.

2. The model

We consider two identical FM leads separated by the insulating layer of thickness d (figure 1). The FM leads have thickness much larger than all other characteristic length scales in the problem. We find magnetic interaction between the leads assuming that s electrons are responsible for magnetic interaction. We assume that magneto-dipole interaction between the leads is absent. The Hamiltonian describing delocalized electrons in the system has the form

$$\begin{aligned}\hat{H} &= \hat{H}_0 + \hat{H}_C, \\ \hat{H}_0 &= \sum_i (\hat{W}_k(\mathbf{r}_i) + \hat{U}_1(\mathbf{r}_i) + \hat{U}_2(\mathbf{r}_i) + \hat{H}_{1m}(\mathbf{r}_i) + \hat{H}_{2m}(\mathbf{r}_i)),\end{aligned}\tag{1}$$

where \hat{H}_0 is the single particle Hamiltonian. The term \hat{W}_k describes the kinetic energy of an electron. Single particle potential energy $\hat{U}_1 = -U\Theta(-z - d/2)$ and $\hat{U}_2 = -U\Theta(z - d/2)$, where the step function $\Theta(z) = 1$, if $z > 0$ and $\Theta(z) = 0$, if $z < 0$. We choose the zero energy level at the top of insulating barrier (see figure 1). $\hat{H}_{1,2m}$ describes the spin subband splitting of delocalized electrons. In the frame of Vonsovskii s-d model such a splitting appears due to exchange interaction of delocalized s electrons with localized d electrons in FM metals [26]. The s-d interaction couples d and s electrons in the same lead and does not produce coupling between the leads. We consider only FM and AFM collinear configurations of the leads magnetizations. Therefore, we have $\hat{H}_{1,2m} = -J_{sd}\hat{\sigma}_z M_{1,2}\Theta(\mp z - d/2)$ (sign “-” stands for the left and “+” for the right leads, respectively), with $M_1 = 1$ and $M_2 = \pm 1$ for FM (“+”) and AFM (“-”) configurations. Note that the spin subband splitting may also appear due to the exchange interaction of s electrons within a lead (see [36]). This coupling renormalizes the s-d coupling constant J_{sd} but also does not lead to the IEC. \hat{H}_C is the Coulomb interaction between conduction s electrons;

In [8, 9] it was demonstrated that the magnetic exchange interaction between FM leads may appear due to the single particle Hamiltonian \hat{H}_0 . The magnetic interaction

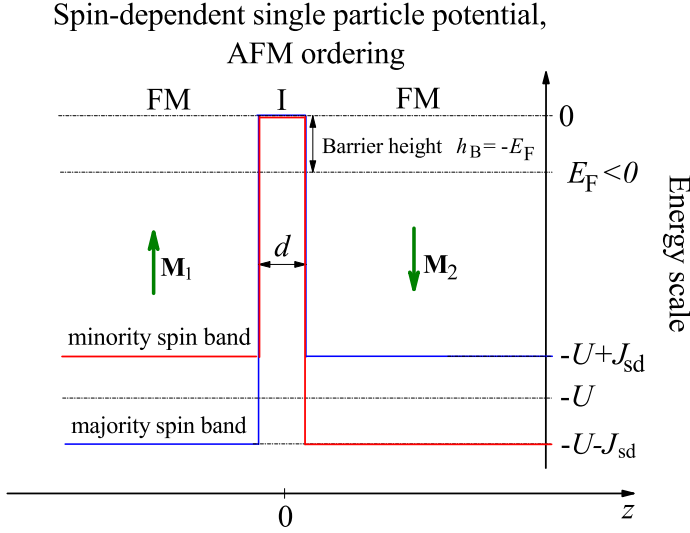


Figure 1. (Color online) Schematic picture of potential energy profiles for electron with spin “up” and “down” states for AFM configuration of leads magnetic moments $\mathbf{M}_{1,2}$. Zero energy corresponds to the top of energy barrier for electrons in the insulator. Symbols FM and I stand for FM metal and insulator, respectively. All other notations are defined in the text.

was considered as a result of spin currents flowing between the leads [8] or as a consequence of varying of electron energy levels density due to interference effects in the insulating layer between the leads [9]. Using perturbation theory we consider the magnetic interaction as a result of virtual electron hopping between the leads [37]. The interlead coupling in Hamiltonian \hat{H}_0 appears as a combination of s-d interaction and the kinetic energy term. The s-d interaction produces the spin polarized s electrons in each lead while the kinetic energy term couples these spin polarized electron gases in the left and the right leads.

It is known that the exchange coupling also exists due to many particle effects. Spin dependent part of the Coulomb interaction couples magnetic moments of two electrons located at different sites with overlapping wave functions (so called Heitler-London model) [27]. Originally this coupling was called the exchange interaction. In this manuscript we consider the spin dependent indirect Coulomb interaction between s electrons located in different layers. Generally, we will sum the interaction of Heitler-London type over all pair of electrons located in different magnetic leads. It leads to the magnetic coupling between the FM layers. This is in contrast to the s-d interaction where d-electrons act on s-electrons in the same layer and do not affect directly the s-electrons in the other lead.

2.1. General procedure of calculation of IEC

We introduce single particle Hamiltonians $\hat{H}_{1,2}$ describing a single lead with infinite insulator

$$\hat{H}_{1,2} = \hat{W}_k + \hat{U}_{1,2} + \hat{H}_{1,2m}. \quad (2)$$

The eigenfunctions of the Hamiltonians are ψ_i^s and ϕ_i^s for leads (1) and (2), respectively. The subscript i stands for orbital state and the superscript s denotes the spin state in the local spin coordinate system related to magnetization in the corresponding lead. The wave functions are symmetric due to symmetry of the problem $\psi_i^s(x, y, z) = \phi_i^s(x, y, -z)$. Energies of these states are ϵ_{1i}^s and ϵ_{2i}^s . For identical leads the energies are equal, $\epsilon_{1i}^s = \epsilon_{2i}^s = \epsilon_i^s$. The creation and annihilation operators in the lead (1) and (2) are \hat{a}_i^{s+} and \hat{a}_i^s , and \hat{b}_i^{s+} and \hat{b}_i^s , respectively.

We introduce the zero-order many-particle wave functions Ψ_0^{AFM} and Ψ_0^{FM} for AFM and FM configurations of leads magnetic moments $\mathbf{M}_{1,2}$ (see wave functions in Appendix A). These wave functions describe the non-interacting FM layers ($d \rightarrow \infty$). All states ψ_i^s and ϕ_j^s with energies $\epsilon_i^s < E_F$ are filled and all states above E_F are empty.

Below we calculate the surface exchange interaction between the FM leads, $H^{\text{ex}} = (E^{\text{AFM}} - E^{\text{FM}})/S$, where E^{AFM} (E^{FM}) is the energy of AFM (FM) state and S is the surface area of the leads. We will assume that the insulator between the leads is thick enough and the interlayer coupling is weak and can be considered within the perturbation theory. The exchange interaction has two contributions: 1) the hopping based exchange interaction, H_h^{ex} - due to the Hamiltonian \hat{H}_0 and 2) the Coulomb based exchange interaction, H_C^{ex} - due to the Hamiltonian \hat{H}_C . The first contribution was calculated in [9]. The second contribution is considered in this paper. When calculating the Coulomb based contribution we neglect corrections to the ground state Ψ_0 due to electron tunnelling between the leads. Validity of this approximation is discussed in the Appendix A. Finally, we use the first order perturbation theory to calculate the indirect Coulomb interaction

$$H_C^{\text{ex}} = \frac{1}{S} (\langle \Psi_0^{\text{AFM}} | \hat{H}_C | \Psi_0^{\text{AFM}} \rangle - \langle \Psi_0^{\text{FM}} | \hat{H}_C | \Psi_0^{\text{FM}} \rangle). \quad (3)$$

We consider (3) in the next sections.

2.2. Estimation of the Hopping based IEC

The hopping based exchange interaction due to Hamiltonian \hat{H}_0 can be estimated as follows. Electron wave functions decay exponentially inside the insulator. Therefore the hopping matrix elements between the leads depend exponentially on distance d as $e^{-\kappa_0 d}$, where $\kappa_0 = \sqrt{-2m_e E_F / \hbar^2}$. These matrix elements are small. The hopping based exchange interaction appears in the second order perturbation theory [37] producing the factor $e^{-2\kappa_0 d}$. Since the hopping based interlead exchange interaction is due to kinetic energy it has the factor $\hbar^2 \kappa_0^2 / (2m_e)$, which always enter the tunnelling matrix elements. In addition, the magnetic coupling between the leads is absent if electron gas inside the

leads is not spin polarized (has no magnetic moment). Therefore, the interlayer coupling is proportional to the spin polarization of s-electrons, $(J_{\text{sd}}/(U + E_{\text{F}}))^2$. Finally, the hopping based IEC can be estimated as follows, $H_{\text{h}}^{\text{ex}} \sim (\hbar^2 \kappa_0^2 / 2m_{\text{e}})(J_{\text{sd}}/(U + E_{\text{F}}))^2 e^{-2\kappa_0 d}$, in a qualitative agreement with [9].

2.3. Estimation of the Coulomb based IEC

Similarly we estimate the s-s Coulomb based exchange interaction between the leads. The matrix element of the indirect Coulomb interaction contains four electron wave functions and therefore is proportional to the square of electron wave functions overlap. The Coulomb based exchange interaction appears in the first order perturbation theory. Therefore, it is also proportional to $e^{-2\kappa_0 d}$. Similar to the hopping based coupling the Coulomb based coupling exists only if electron gas in each lead is spin-polarized producing the factor $(J_{\text{sd}}/(U + E_{\text{F}}))^2$. In addition, the Coulomb interaction between two electrons inside the barrier can be estimated as $e^2/(\varepsilon d)$, where ε is the insulator dielectric constant. Combining all these factors the Coulomb based exchange coupling can be estimated as follows, $H_{\text{C}}^{\text{ex}} \sim (e^2/\varepsilon d)(J_{\text{sd}}/(U + E_{\text{F}}))^2 e^{-2\kappa_0 d}$.

For interlayer distance $d = 1$ nm, barrier height $h_{\text{B}} = -E_{\text{F}} = 0.2$ eV, and $\varepsilon = 5$ the hopping and the Coulomb based exchange contributions are comparable. Therefore the Coulomb based exchange coupling is important and should be taken into account in this problem.

3. Main results

Our main findings are the following:

1) We calculate the exchange coupling in MTJ due to Coulomb interaction between s electrons located at different leads. We show that the Coulomb based IEC can exceed the hopping based exchange contribution studied by Slonczewski, Bruno and Jullier in the past. We find that these two mechanisms have essentially different dependence on system parameters (see figures 2, 3, 4, 5, 6).

2) We find that the hopping and the Coulomb based exchange interaction have the same small factor due to weak wave functions overlap, $e^{-2\kappa_0 d}$. In addition, both contributions have similar dependence on the s-d coupling constant. For small spin subband splitting both contributions are proportional to $(J_{\text{sd}}/(U + E_{\text{F}}))^2$. The hopping based IEC is related to the kinetic energy term in the system Hamiltonian and therefore has the factor $\hbar^2 \kappa_0^2 / (2m_{\text{e}})$. The Coulomb based exchange contribution is due to electric forces acting between s-electrons, as a result it has the factor $e^2/(\varepsilon d)$.

3) We find the approximate analytical expressions for the Coulomb (H_{C}^{ex}) and the hopping (H_{h}^{ex}) based IEC per unit area in the limit $J_{\text{sd}} \ll (U + E_{\text{F}})$, $\kappa_0 \ll k_{\text{F}}$ ($k_{\text{F}} = \sqrt{2m_{\text{e}}(U + E_{\text{F}})/\hbar^2}$)

$$H_{\text{h}}^{\text{ex}} \approx -\frac{2\hbar^2}{\pi^2 m_{\text{e}} d^2} \frac{J_{\text{sd}}^2}{(U + E_{\text{F}})^2} \frac{\kappa_0^5}{k_{\text{F}}^3} e^{-2\kappa_0 d}, \quad (4)$$

$$H_C^{\text{ex}} \approx \frac{\zeta e^2}{4\pi\epsilon_0\epsilon d} \frac{J_{\text{sd}}^2}{(U + E_F)^2} \frac{k_F}{d} e^{-2\kappa_0 d}, \quad (5)$$

where $\zeta \approx 1/150$.

4) We show that in contrast to hopping based exchange interaction, the Coulomb based exchange is inversely proportional to the dielectric constant ϵ of the insulating layer (see figure 7).

5) We calculate the IEC as a function of temperature and electric field (or voltage across the MTJ) for MTJ with insulating layer made of tetrathiafulvalene p-chloranil complex (TTF-CA) and $\text{Hf}_{0.5}\text{Zr}_{0.5}\text{O}_2$ (see figures 8, 9). We show that in the vicinity of the FE phase transition of TTF-CA the IEC has large variations. We find that even the FM-AFM transition may occur in MTJ for some system parameters.

6) We find that IEC as a function of electric field (or applied voltage) shows strong variations. The electric field can cause the transition from AFM to FM coupling: for zero field the coupling is AFM while for finite field it is FM. This effect demonstrates the ME coupling in MTJ.

4. Basic wave functions

We use the coordinate system with z -axis being perpendicular to the leads surfaces and x and y being perpendicular to z , $r_\perp = \sqrt{x^2 + y^2}$. In the absence of spin-orbit interaction the spin and the spatial parts of wave functions are decoupled. The spin parts are $(1 \ 0)^T$ and $(0 \ 1)^T$ for the spin up and spin down states, respectively. The spatial part of electron wave functions inside the leads consists of two plane waves: one going toward the leads surface and the other being reflected from the FM/insulator interface

$$\begin{aligned} \psi_i^s(z, \mathbf{r}_\perp) &= \frac{e^{ik_z(\frac{d}{2}+z)} + \xi_{\mathbf{k}}^s e^{-ik_z(\frac{d}{2}+z)}}{\sqrt{\Omega}} e^{i\mathbf{k}_\perp \mathbf{r}_\perp}, \quad z < -d/2 \\ \phi_i^s(z, \mathbf{r}_\perp) &= \frac{e^{ik_z(\frac{d}{2}-z)} + \xi_{\mathbf{k}}^s e^{-ik_z(\frac{d}{2}-z)}}{\sqrt{\Omega}} e^{i\mathbf{k}_\perp \mathbf{r}_\perp}, \quad z > d/2, \end{aligned} \quad (6)$$

where $\xi_{\mathbf{k}}^s = \frac{k_z - i\kappa_{\mathbf{k}}^s}{k_z + i\kappa_{\mathbf{k}}^s}$ is the amplitude of the reflected electron wave, with $\kappa_{\mathbf{k}}^s = \sqrt{2m_e(U - sJ_{\text{sd}})/\hbar^2 - k_z^2}$. Superscript i denotes the full set of quantum numbers (k_x, k_y, k_z) , $\mathbf{k}_\perp = (k_x, k_y, 0)$ and $\mathbf{r}_\perp = (x, y, 0)$ and Ω is the volume of each lead.

In the region $z > -d/2$ we have for the wave function of the left lead

$$\psi_i^s(z, r_\perp) = \frac{\tau_{\mathbf{k}}^s}{\sqrt{\Omega}} e^{-\kappa_{\mathbf{k}}^s(\frac{d}{2}+z)} e^{i\mathbf{k}_\perp \mathbf{r}_\perp}, \quad z > -d/2, \quad (7)$$

where $\tau_{\mathbf{k}}^s = \frac{2k_z}{k_z + i\kappa_{\mathbf{k}}^s}$ is the amplitude of the transmitted electron wave. The electron wave function for the states in the right lead for $z < d/2$ is

$$\phi_i^s(z, r_\perp) = \frac{\tau_{\mathbf{k}}^s}{\sqrt{\Omega}} e^{-\kappa_{\mathbf{k}}^s(\frac{d}{2}-z)} e^{i\mathbf{k}_\perp \mathbf{r}_\perp}, \quad z < d/2. \quad (8)$$

Note that ψ and ϕ are the wave functions of isolated leads ($d \rightarrow \infty$). Therefore, these wave functions decay exponentially in the region $z > -d/2$ for the left lead states and

$z < d/2$ for the right lead states. This is in contrast to Bruno (or Slonczewski) model for hopping based IEC, where the wave functions of states in the left lead have oscillating part in the right lead and vice versa. In our consideration we neglect tunnelling when calculating the Coulomb based IEC. We discuss this point in more details in Appendix A.

5. Exchange due to Coulomb interaction

Both terms in (3) have contributions from direct and indirect Coulomb interaction. The direct Coulomb interaction does not lead to the spin-dependent correction to the system energy and will be omitted below. Also we will omit the indirect Coulomb interaction between conduction electrons in the same lead. On one hand this contribution does not lead to the interaction between the leads and on the other hand it leads to spin subband splitting which is much smaller than the splitting due to the s-d interaction.

We assume that IEC is small due to large distance between the leads and weak overlap of electron wave functions. Therefore we use the first order perturbation theory to study this coupling. We average the Coulomb operator, \hat{H}_C , over the ground state of unperturbed (non-interacting) system. We use the local coordinate spin system with z-axis being co-directed with lead magnetic moment. Therefore, the operator of Coulomb interaction is different for FM and AFM orientations of leads magnetic moments. The reduced Hamiltonian takes into account only interaction between electrons at different leads and has the form

$$\hat{H}_C^{\text{ex}} = \begin{cases} -\sum_{i,j,s} U_{ijj}^{\text{ss}} \hat{a}_i^{s+} \hat{a}_i^s \hat{b}_j^{s+} \hat{b}_j^s, & \text{FM ordering,} \\ -\sum_{i,j,s} \tilde{U}_{ijj}^{\text{ss}} \hat{a}_i^{s+} \hat{a}_i^s \hat{b}_j^{-s+} \hat{b}_j^{-s}, & \text{AFM ordering,} \end{cases} \quad (9)$$

The operator does not include the factor 1/2 because we sum over the equal elements ($U_{ijkl}^{s1s2} \hat{a}_i^{s1+} \hat{a}_j^{s2} \hat{b}_k^{s2+} \hat{b}_l^{s1}$) and ($U_{jilk}^{s1s2} \hat{a}_k^{s2+} \hat{a}_l^{s1} \hat{b}_i^{s1+} \hat{b}_j^{s2}$).

The electron wave function has a random phase due to scattering on impurities therefore only the diagonal matrix elements of exchange interaction contribute to the system energy, $U_{iikk}^{s1s2} \neq 0$. Below we will omit the double subscripts and superscripts for matrix elements of the Coulomb interaction. The matrix element has the form [27]

$$\begin{aligned} U_{ij}^s &= \frac{1}{S} \iint d^3\mathbf{r}_1 d^3\mathbf{r}_2 \psi_i^{s*}(\mathbf{r}_1) \phi_j^s(\mathbf{r}_1) \hat{U}_C \psi_i^s(\mathbf{r}_2) \phi_j^{s*}(\mathbf{r}_2), \\ \tilde{U}_{ij}^s &= \frac{1}{S} \iint d^3\mathbf{r}_1 d^3\mathbf{r}_2 \psi_i^{s*}(\mathbf{r}_1) \phi_j^{-s}(\mathbf{r}_1) \hat{U}_C \psi_i^s(\mathbf{r}_2) \phi_j^{-s*}(\mathbf{r}_2), \end{aligned} \quad (10)$$

where \hat{U}_C is the operator of the Coulomb interaction. For homogeneous insulator it has the form $\hat{U}_C = e^2/(4\pi\epsilon_0\epsilon|\mathbf{r}_1 - \mathbf{r}_2|)$, where ϵ is the medium effective dielectric constant. In our case the system is inhomogeneous and the Coulomb interaction is renormalized due to screening effects due to presence of metallic leads.

The right hand side of (10) can be considered as the Coulomb interaction between two effective charges, $\rho_{ij}^{(1)} = e\psi_i^{s*}(\mathbf{r})\phi_j^{s'}(\mathbf{r})$ and $\rho_{ij}^{(2)} = e\psi_i^s(\mathbf{r})\phi_j^{s'*}(\mathbf{r})$. Here we use $s' = s$ for FM and $s' = -s$ for AFM configurations.

The wave functions of two electrons located at different leads ψ_i and ϕ_j are overlapped inside the insulating layer and inside the leads. Therefore, there are two regions contributing to (10):

1) The region inside the FM leads Ω_1 (Ω_2) where the Coulomb interaction is effectively screened and is short-range [36]

$$\hat{U}_C^L = \frac{\Omega\Delta}{2}\delta(\mathbf{r}_1 - \mathbf{r}_2), \quad (11)$$

where Δ is the mean energy level spacing, $\Omega\Delta = 6\pi^2 E_F / ((k_F^+)^3 + (k_F^-)^3)$, with the Fermi momentum $k_F^s = \sqrt{2m_e(U + E_F - sJ_{sd})/\hbar^2}$. The peculiarity of this term is related to the fact that it does not depend on dielectric properties of insulating layer. This region gives the following contribution

$$L_{ij}^s = \frac{1}{S} \int \int_{\Omega_1 + \Omega_2} d^3\mathbf{r}_1 d^3\mathbf{r}_2 \psi_i^{s*}(\mathbf{r}_1) \phi_j^s(\mathbf{r}_1) \hat{U}_C^L \psi_i^s(\mathbf{r}_2) \phi_j^{s*}(\mathbf{r}_2), \quad (12)$$

where $\Omega_{1,2} = \Omega$ is the lead volume.

2) The second region contributing to (10) is the region between the leads where screening of the Coulomb interaction is weak and the interaction is long-range. However, due to metallic leads, the electric field of two interacting electrons is finite only inside this region. We denote the renormalized Coulomb interaction inside the insulating layer as \hat{U}_C^I . This contribution depends on the dielectric permittivity ε of the insulating layer. This region gives the following contribution

$$I_{ij}^s = \frac{1}{S} \int \int_{\Omega_I} d^3\mathbf{r}_1 d^3\mathbf{r}_2 \psi_i^{s*}(\mathbf{r}_1) \phi_j^s(\mathbf{r}_1) \hat{U}_C^I \psi_i^s(\mathbf{r}_2) \phi_j^{s*}(\mathbf{r}_2), \quad (13)$$

where Ω_I is the volume of the insulating layer. We can write the matrix elements of the indirect Coulomb interaction as a sum of two terms. For FM ordering we have

$$U_{ij}^s = L_{ij}^s + I_{ij}^s. \quad (14)$$

Note that electrons inside the insulator and electrons inside the leads are decoupled and do not interact with each other. Therefore, there are no terms with integration over the \mathbf{r}_1 in the region Ω_I and over the \mathbf{r}_2 in the regions $\Omega_{1,2}$ ($\int_{\Omega_I} d^3\mathbf{r}_1 \int_{\Omega_{1,2}} d^3\mathbf{r}_2$).

Similarly we can write the matrix elements for AFM state \tilde{U}_{ij}^s . We can split the total IEC based on the Coulomb interaction into two contributions

$$H_C^{\text{ex}} = L^{\text{ex}} + I^{\text{ex}}. \quad (15)$$

Below we consider these two contributions to the Coulomb based exchange interaction separately.

5.1. Contribution to the exchange interaction due to the insulating region, I^{ex}

This contribution includes three terms: 1) \tilde{I}_{ex}^- - FM configuration, majority spin subband; 2) \tilde{I}_{ex}^+ - FM configuration, minority spin subband; 3) \tilde{I}_{ex} - AFM configuration (both spin subbands give the same contribution in AFM case).

Consider the first term \tilde{I}_{ex}^- . Replacing summation in (9) with integration we have

$$\tilde{I}_{\text{ex}}^- = -\frac{\Omega^2}{(2\pi)^6 S} \int \int_{\epsilon_1^-, \epsilon_2^- < E_F} d^3 k_1 d^3 k_2 I_{\mathbf{k}_1 \mathbf{k}_2}^-, \quad (16)$$

where $\epsilon^s = \hbar^2 k^2 / (2m_e) + sJ_{\text{sd}} + U$. Substituting (7) and (8) into (16) we obtain

$$\begin{aligned} \tilde{I}_{\text{ex}}^- &= \frac{-\Omega^2}{(2\pi)^6 S} \int d^3 r_1 d^3 r_2 d^3 k_1 d^3 k_2 \hat{U}_C^1(\mathbf{r}_1, \mathbf{r}_2) \times \\ &\times \rho(z_1)(\rho(z_2))^* e^{i(\mathbf{k}_{1\perp} - \mathbf{k}_{2\perp})\mathbf{r}_{1\perp}} e^{-i(\mathbf{k}_{1\perp} - \mathbf{k}_{2\perp})\mathbf{r}_{2\perp}}, \end{aligned} \quad (17)$$

where

$$\rho(z) = \frac{e\tau_i^{s*}\tau_j^s}{\Omega} e^{-z(\varkappa_i^s - \varkappa_j^s)} e^{-\frac{d}{2}(\varkappa_i^s + \varkappa_j^s)}. \quad (18)$$

The integral over $\mathbf{r}_{1,2}$ describes the interaction energy of two effective charges. The effective charges decay exponentially along z direction and harmonically vary in the transverse direction. The effective charges produce an electric field. This field is screened by metallic leads and is finite only inside the insulating layer. The details of calculations are shown in Appendix B. The final result for \tilde{I}_{ex}^- has the form

$$\begin{aligned} \tilde{I}_{\text{ex}}^- &= -\frac{e^2}{32\pi^4 \varepsilon_0 \varepsilon} \int_0^{k_F^-} \int_0^{k_1} dk_1 dk_2 |(\tau_1^-)^* \tau_2^-|^2 e^{-d(\varkappa_1^- + \varkappa_2^-)} \times \\ &\times \int_0^{k_2^{\text{max}} + k_1^{\text{max}}} q\omega_1(q) dq \int_0^{(k_2^{\text{max}} + k_1^{\text{max}})/2} k\zeta(k, q) dk, \end{aligned} \quad (19)$$

where \varkappa in the expression for $\omega_1(q)$ (B.18) is taken for majority ($s = "-"$) spin subband and we introduce the notation $k_1^{\text{max}} = \sqrt{(k_F^-)^2 - k_{1z}^2}$ and $k_2^{\text{max}} = \sqrt{(k_F^-)^2 - k_{2z}^2}$. The functions $\omega_1(q)$ and $\zeta(k, q)$ are defined in Appendix B.

The contribution from the minority ($s = "+"$) spin subband has the form

$$\begin{aligned} \tilde{I}_{\text{ex}}^+ &= -\frac{e^2}{32\pi^4 \varepsilon_0 \varepsilon} \int_0^{k_F^+} \int_0^{k_1} dk_1 dk_2 |(\tau_1^+)^* \tau_2^+|^2 e^{-d(\varkappa_1^+ + \varkappa_2^+)} \times \\ &\times \int_0^{k_2^{\text{max}} + k_1^{\text{max}}} q\omega_1(q) dq \int_0^{(k_2^{\text{max}} + k_1^{\text{max}})/2} k\zeta(k, q) dk. \end{aligned} \quad (20)$$

We use \varkappa for minority spin subband in the expression for $\omega_1(q)$ and $k_{1,2}^{\text{max}}$ should be taken for minority spin subband ($k_F^- \rightarrow k_F^+$).

Similarly we calculate the contribution due to AFM configuration

$$\begin{aligned} \tilde{\tilde{I}}_{\text{ex}} &= -\frac{e^2}{32\pi^4 \varepsilon_0 \varepsilon} \int_0^{k_F^+} \int_0^{k_F^-} dk_1 dk_2 |(\tau_1^+)^* \tau_2^-|^2 e^{-d(\varkappa_1^+ + \varkappa_2^-)} \times \\ &\times \int_0^{k_2^{\text{max}} + k_1^{\text{max}}} q\omega_1(q) dq \int_0^{(k_2^{\text{max}} + k_1^{\text{max}})/2} k\zeta(k, q) dk. \end{aligned} \quad (21)$$

Here we use \varkappa_2 for majority spin subband and \varkappa_1 for minority spin subband in the expression for ω_1 . Similarly, we have $k_1^{\text{max}} = \sqrt{(k_F^+)^2 - k_{1z}^2}$ and $k_2^{\text{max}} = \sqrt{(k_F^-)^2 - k_{2z}^2}$. The contributions to the energy of AFM configuration from both spin subbands are equal and were included into $\tilde{\tilde{I}}_{\text{ex}}$. Using (19-21) we find the total contribution to the exchange interaction due to the insulating region

$$I^{\text{ex}} = \tilde{\tilde{I}}_{\text{ex}} - \tilde{I}_{\text{ex}}^+ - \tilde{I}_{\text{ex}}^-. \quad (22)$$

5.2. Contribution to the exchange interaction due to the FM leads, L^{ex}

Inside the metallic leads the Coulomb interaction is short-range therefore the matrix element of the exchange interaction has the form

$$L_{ij}^s = \frac{\Omega\Delta}{2S} \int_{\Omega_1+\Omega_2} d^3\mathbf{r} |\psi_i^s(\mathbf{r})|^2 |\phi_j^{s'}(\mathbf{r})|^2, \quad (23)$$

where $s' = s$ for FM and $s' = -s$ for AFM states. Using (6) and (7) we obtain for normalized matrix element the following result

$$\begin{aligned} L_{ij}^s &= \frac{\Delta|\tau_j^s|^2 e^{-2d\kappa_j^s}}{\Omega} \left(\frac{1 + |\xi_i^{s'}|^2}{2\kappa_j^s} + \text{Re} \left(\frac{(\xi_i^{s'})^*}{\kappa_j^s + ik_i} \right) \right) + \\ &\frac{\Delta|\tau_i^{s'}|^2 e^{-2d\kappa_i^{s'}}}{\Omega} \left(\frac{1 + |\xi_j^s|^2}{2\kappa_i^{s'}} + \text{Re} \left(\frac{(\xi_j^s)^*}{\kappa_i^{s'} + ik_j} \right) \right). \end{aligned} \quad (24)$$

Integrating this matrix element over all eigenstates of the ground state we find for FM configuration

$$\begin{aligned} \tilde{L}_{\text{ex}}^s &= \frac{3(U + E_F)}{2^6 \pi ((k_F^+)^3 + (k_F^-)^3)} \times \\ &\times \int_0^{k_F^s} dk_1 \int_0^{k_F^s} dk_2 ((k_F^s)^2 - k_2^2)((k_F^s)^2 - k_1^2) \times \\ &\times \left\{ e^{-2d\kappa_1^s} |\tau_1^s|^2 \left(\frac{1 + |\xi_2^s|^2}{2\kappa_1^s} + \text{Re} \left(\frac{(\xi_2^s)^*}{\kappa_1^s + ik_2} \right) \right) + \right. \\ &\left. |\tau_2^s|^2 e^{-2d\kappa_2^s} \left(\frac{1 + |\xi_1^s|^2}{2\kappa_2^s} + \text{Re} \left(\frac{(\xi_1^s)^*}{\kappa_2^s + ik_1} \right) \right) \right\}, \end{aligned} \quad (25)$$

and for AFM configuration we have

$$\begin{aligned} \tilde{L}_{\text{ex}} &= \frac{6(U + E_F)}{2^6 \pi ((k_F^+)^3 + (k_F^-)^3)} \times \\ &\times \int_0^{k_F^+} dk_1 \int_0^{k_F^-} dk_2 ((k_F^-)^2 - k_2^2)((k_F^+)^2 - k_1^2) \times \\ &\times \left\{ e^{-2d\kappa_1^+} |\tau_1^+|^2 \left(\frac{1 + |\xi_2^-|^2}{2\kappa_1^+} + \text{Re} \left(\frac{(\xi_2^-)^*}{\kappa_1^+ + ik_2} \right) \right) + \right. \\ &\left. |\tau_2^-|^2 e^{-2d\kappa_2^-} \left(\frac{1 + |\xi_1^+|^2}{2\kappa_2^-} + \text{Re} \left(\frac{(\xi_1^+)^*}{\kappa_2^- + ik_1} \right) \right) \right\}. \end{aligned} \quad (26)$$

Using (25) and (26) we find the total contribution to the exchange interaction due to the leads

$$L^{\text{ex}} = \tilde{L}_{\text{ex}} - \tilde{L}_{\text{ex}}^+ - \tilde{L}_{\text{ex}}^-. \quad (27)$$

5.3. Total exchange interaction

The total exchange interaction is given by the expression

$$H^{\text{ex}} = H_{\text{h}}^{\text{ex}} + \tilde{L}_{\text{ex}} - \tilde{L}_{\text{ex}}^+ - \tilde{L}_{\text{ex}}^- + \tilde{L}_{\text{ex}} - \tilde{L}_{\text{ex}}^+ - \tilde{L}_{\text{ex}}^-. \quad (28)$$

The first term was calculated in [9]

$$H_h^{\text{ex}} = -\frac{\hbar^2}{\pi^2 m_e d^2} \varkappa_0^5 b e^{-2\varkappa_0 d}, \quad (29)$$

$$b = \begin{cases} \frac{(\varkappa_0^2 - k_F^+ k_F^-)(k_F^+ - k_F^-)^2 (k_F^+ + k_F^-)}{(\varkappa_0^2 + (k_F^+)^2)^2 (\varkappa_0^2 + (k_F^-)^2)^2}, & U + E_F > J_{\text{sd}}, \\ \frac{k_F^- ((k_F^-)^2 + i\varkappa_0 k_F^+)}{\varkappa_0 (\varkappa_0^2 + (k_F^-)^2)^2 (\varkappa_0 - i k_F^+)}, & U + E_F < J_{\text{sd}}. \end{cases}$$

Here the coefficient b is always real. For $U + E_F < J_{\text{sd}}$ (the second line) the Fermi momentum k_F^+ is imaginary, $k_F^+ = i|k_F^+|$.

5.4. Half metals

For half metals with one spin subband ($U + E_F < J_{\text{sd}}$) the first contribution in (3) is absent and only the majority spin subband contributes to the second term in (3).

5.5. Analytical expression for limiting case

For weak spin subband splitting, $J_{\text{sd}} \ll (U + E_F)$ and large decay length, $\varkappa_0 \ll k_F$, the IEC is quadratic in J_{sd} and can be written in powers of small parameter \varkappa_0/k_F . In the leading order we find

$$H_h^{\text{ex}} \approx -\frac{2\hbar^2}{\pi^2 m_e d^2} \frac{J_{\text{sd}}^2}{(U + E_F)^2} \frac{\varkappa_0^5}{k_F^3} e^{-2\varkappa_0 d}, \quad (30)$$

and for the Coulomb based IEC we have

$$H_C^{\text{ex}} \approx \frac{\zeta e^2}{4\pi\epsilon_0\epsilon d} \frac{J_{\text{sd}}^2}{(U + E_F)^2} \frac{k_F}{d} e^{-2\varkappa_0 d}, \quad (31)$$

with $\zeta \approx 1/150$. The expression for the Coulomb based IEC is derived by fitting (3). In this limit the Coulomb based contribution gives the largest contribution to the IEC.

6. Discussion of results

6.1. Comparison of three contributions to the total exchange interaction

We split the total exchange interaction into three components H_h^{ex} , L^{ex} and I^{ex} . These contributions have different origins and behavior. The first contribution, H_h^{ex} , appears due to spin current between the leads. The second, L^{ex} , and the third, I^{ex} , contributions are due to many-body effects. It is important that I^{ex} depends on the dielectric permittivity of the insulating layer in contrast to the first and the second contributions.

Figure 2 shows the dependence of three contributions on the barrier height h_B , in our notations $h_B = -E_F$, for the following parameters: $U = 5$ eV, $d = 1$ nm, $\epsilon = 4.5$, $J_{\text{sd}} = 5.2; 4.5; 4.0$ eV. All three contributions have different behavior as a function of barrier height h_B . For large spin subband splitting, J_{sd} (half metals) shown in figure 2(a) all three contributions do not change their sign as a function of h_B . The Coulomb based IEC is positive while the hopping based one is negative. For small J_{sd} (two spin

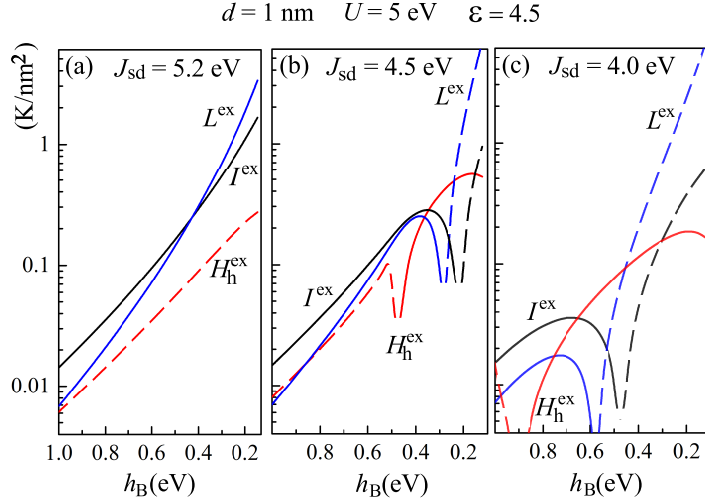


Figure 2. (Color online) The interlayer exchange interaction as a function of insulating barrier height h_B for $U = 5 \text{ eV}$, $\varepsilon = 4.5$, $d = 1 \text{ nm}$ and (a) $J_{sd} = 5.2 \text{ eV}$, (b) $J_{sd} = 4.5 \text{ eV}$, (c) $J_{sd} = 4 \text{ eV}$. Black lines show $|I^{\text{ex}}|$ (22), blue lines are for $|L^{\text{ex}}|$ (27) and red lines are for $|H_h^{\text{ex}}|$ (29). The y-axis has logarithmic scale. Dashed parts show the region where functions I^{ex} , L^{ex} and H_h^{ex} are negative.

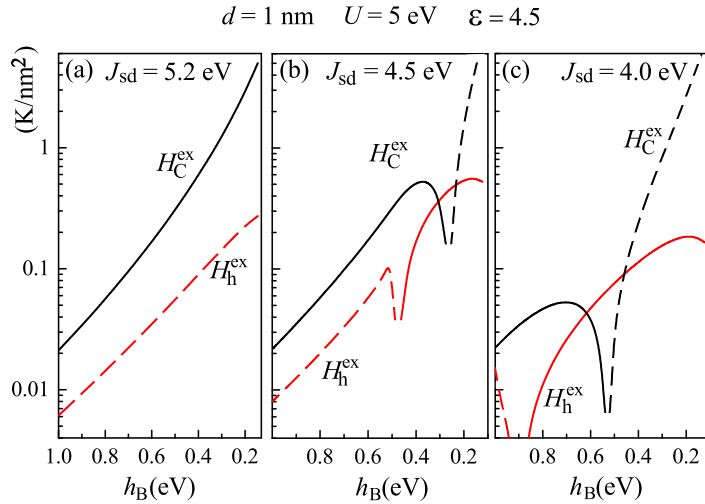


Figure 3. (Color online) The interlayer exchange interaction as a function of h_B for $U = 5 \text{ eV}$, $\varepsilon = 4.5$, $d = 1 \text{ nm}$ and (a) $J_{sd} = 5.2 \text{ eV}$, (b) $J_{sd} = 4.5 \text{ eV}$, (c) $J_{sd} = 4 \text{ eV}$. Black lines are for $|H_C^{\text{ex}}|$ (15), and red lines are for $|H_h^{\text{ex}}|$ (29). Dashed parts show the region where functions H_C^{ex} and H_h^{ex} are negative.

subband metals) all three contributions are non-monotonic and change their sign and can be either of FM or AFM type depending on the barrier height. The contribution I^{ex} (black line) depends on the dielectric permittivity of the insulating layer in contrast to two other contributions. We use SiO_2 with $\varepsilon = 4.5$ as an example. For insulators with high dielectric constants $\varepsilon > 100$ this contribution is suppressed.

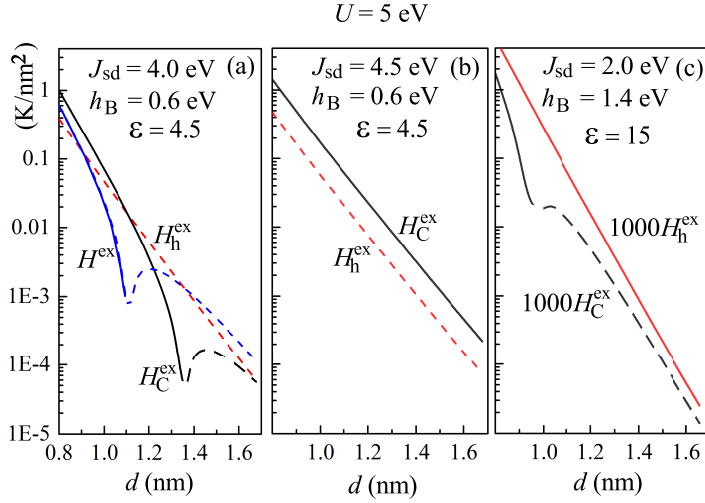


Figure 4. (Color online) The interlayer exchange interaction as a function of the insulator thickness d for $U = 5$ eV, and (a) $J_{sd} = 4.0$ eV, $h_B = 0.6$ eV, $\varepsilon = 4.5$, (b) $J_{sd} = 4.5$ eV, $h_B = 0.6$ eV, $\varepsilon = 4.5$, (c) $J_{sd} = 2.0$ eV, $h_B = 1.4$ eV, $\varepsilon = 15$. Black lines are for $|H_C^{\text{ex}}|$ (15), red lines are for $|H_h^{\text{ex}}|$ (29), blue line is for total exchange interaction, H^{ex} (28). Dashed parts show the region where functions are negative.

Figure 2 shows that all three contributions to the IEC are comparable and there is no a single component dominating in the whole range of parameters, especially if we take into account the fact that all three components change their sign at different values of barrier height. For strong subband splitting (half metal) and $\varepsilon < 4$ the Coulomb based contribution dominates for any barrier heights. This contribution also dominates for small spin subband splitting in the region of high barrier height ($h_B > 0.3$ eV for $J_{sd} = 4.5$ eV and $h_B > 0.6$ eV for $J_{sd} = 4.0$ eV). For spin subband splitting smaller than the average conduction band width, $W_{\text{con}} = U + E_F$, and for low barrier height ($h_B < 0.3$ eV in figure 2) the Coulomb based exchange interaction, L^{ex} provides the main contribution to the IEC. For spin subband splitting smaller than the average conduction band width, W_{con} there is also a region where the hopping based exchange interaction, H_h^{ex} dominates. Using the fact that I^{ex} depends on the dielectric constant, in experiment one can have any relation between these three contributions.

Figure 3 shows the dependence of the total Coulomb based exchange contribution, $H_C^{\text{ex}} = I^{\text{ex}} + L^{\text{ex}}$ and the hopping based contribution, H_h^{ex} as a function of barrier height, h_B . For half-metal (panel (a)) the contributions H_h^{ex} and H_C^{ex} have the opposite sign for any h_B . Also for full metal ($J_{sd} < U + E_F$) the hopping and the Coulomb based contributions have the opposite sign. However, the FM/AFM transitions appear at different barrier height, h_B . The FM/AFM transition point of the Coulomb based contribution is located above the transition point of the hopping based exchange. The Coulomb based exchange mostly exceeds the hopping based exchange. Only in the vicinity of the FM/AFM transition point of H_C^{ex} the hopping based exchange dominates.

Figure 4 shows the behavior of the IEC as a function of the insulator thickness d for

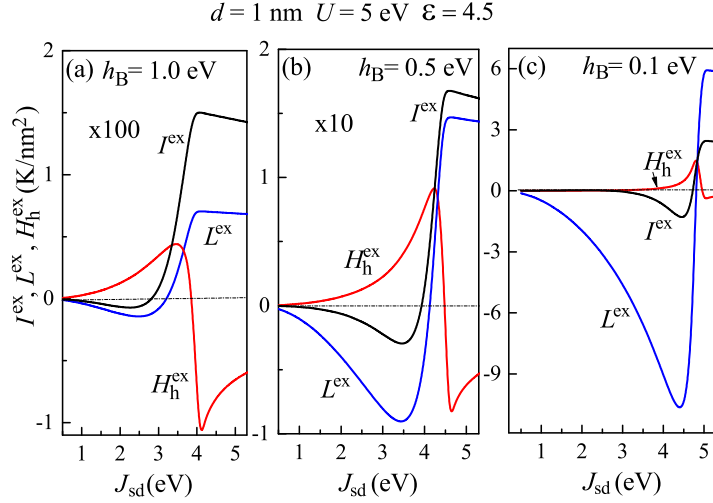


Figure 5. (Color online) The interlayer exchange interaction as a function of spin subband splitting, J_{sd} , for $U = 5$ eV, $\varepsilon = 4.5$, $d = 1$ nm, and (a) $h_B = 1.0$ eV, (b) $h_B = 0.5$ eV, (c) $h_B = 0.1$ eV. Black lines are for I^{ex} (22), blue line is for L^{ex} (27), and red lines are for H_h^{ex} (29). The data are multiplied by 100 in panel (a) and by 10 in panel (b).

the following parameters $U = 5$ eV, $\varepsilon = 4.5$; 15. The Coulomb and the hopping based contributions are shown separately. The total exchange interaction is also shown. The barrier height and the spin subband splitting is different for different panels. Panel (b) ($J_{sd} = 4.5$ eV and $h_B = 0.6$ eV, half-metal leads) shows the case where the Coulomb exchange dominates. In this case the exchange coupling decays exponentially with thickness d and has the same decay rate as the hopping based exchange ($e^{-2d\kappa_0}/d^2$). Therefore the dependence on thickness does not allow to distinguish the Coulomb and the hopping based exchange contributions.

Panel (c) ($J_{sd} = 2.0$ eV and $h_B = 1.4$ eV, two spin subband metal) shows the opposite situation when the hopping based exchange coupling dominates. Figure 4(a) ($J_{sd} = 4$ eV, $h_B = 0.6$ eV) shows the case when both contributions are of the same order. In this situation the Coulomb based exchange interaction has a more complicated behavior which is substantially different from the behavior of the hopping based exchange contribution. At some thickness the Coulomb based contribution changes its sign. For small thickness the Coulomb based contribution H_C^{ex} is positive (FM) while the hopping based exchange is negative (AFM). For large thickness both contributions are of AFM type. The blue curve shows the total IEC. One can see that H^{ex} also changes its sign. Such a behavior is due to competition of two contributions. The Coulomb based exchange interaction can be studied using this non-monotonic behavior.

Figure 5 shows the dependence of the exchange coupling on the spin subband splitting J_{sd} for $U = 5$ eV, $\varepsilon = 4.5$, $d = 1$ nm, and $h_B = 1.0; 0.5; 0.1$ eV. These plots show that contribution I^{ex} dominates if only one spin subband is filled ($J_{sd} > U + E_F$). For

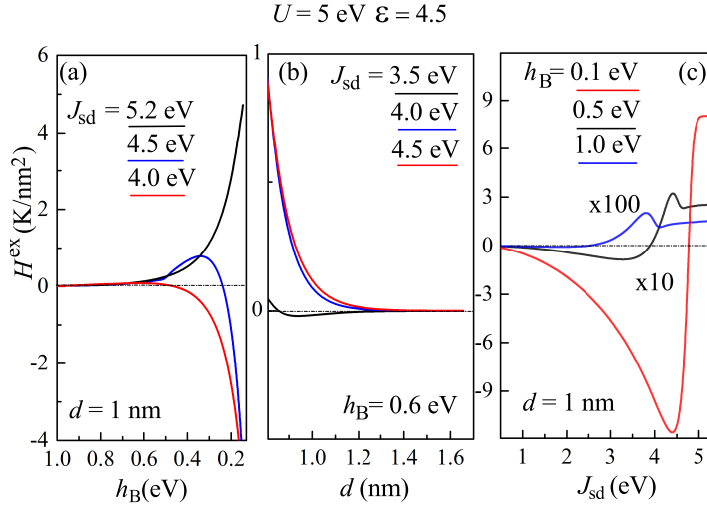


Figure 6. (Color online) Total interlayer exchange coupling (IEC), H^{ex} in (28) as a function of (a) barrier height h_B ; (b) barrier thickness d ; (c) and the spin subband splitting J_{sd} for $U = 5$ eV, $\varepsilon = 4.5$. In panel (c) the data for $h_B = 1.0$ eV are multiplied by 100 and for $h_B = 0.5$ eV by 10.

small splitting the main contribution is due to hopping, H_h^{ex} and the Coulomb based, L^{ex} exchange. Figure 5 shows that transition from FM to AFM coupling for different contributions appears at different values of the spin subband splitting, J_{sd} . In addition, the behavior of all contributions strongly depends on the barrier height.

6.2. Total IEC vs spin subband splitting J_{sd} , barrier height h_B and insulator thickness d

Figure 6 shows the total IEC, H^{ex} in (28) as a function of barrier height h_B , barrier thickness d , and the spin subband splitting J_{sd} for $U = 5$ eV, $\varepsilon = 4.5$. These curves show that H^{ex} decays with the thickness of the insulating layer and decays with increasing the barrier height. For small spin subband splitting the coupling is weak and negative (AFM). For large subband splitting the IEC becomes FM (positive) and reaches its maximum value. The important feature of the Coulomb based exchange coupling is its dependence on the dielectric constant ε of insulator layer. The hopping based exchange coupling does not depend on ε .

6.3. Coulomb based exchange coupling vs dielectric permittivity of the insulating layer: ME effect

The important feature of the Coulomb based exchange interaction is its dependence on the dielectric permittivity ε of the insulating layer. The Coulomb based exchange interaction has two contributions: 1) The indirect Coulomb interaction inside the leads - L^{ex} in (27). This term does not depend on the properties of the insulating layer. 2) The indirect Coulomb interaction inside the insulating layer - I^{ex} in (22). This term is inversely proportional to the dielectric constant of the insulating layer, $I^{\text{ex}} \sim \varepsilon^{-1}$. To

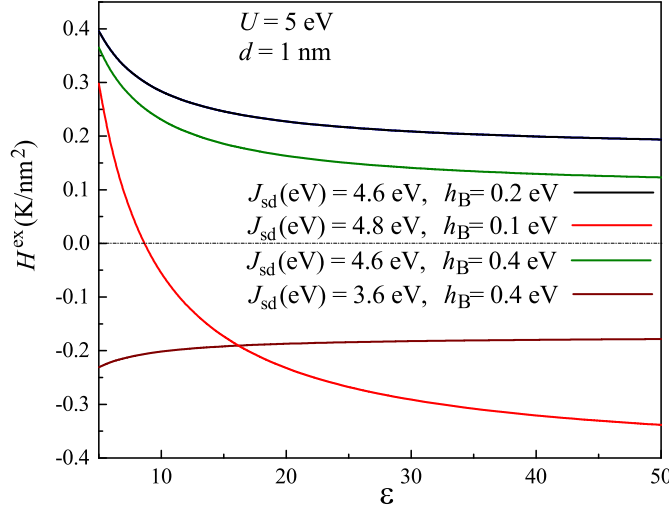


Figure 7. (Color online) Total interlayer exchange coupling (IEC), H^{ex} in (28) as a function of dielectric permittivity of the insulating layer, ε , for $U = 5$ eV, $d = 1$ nm and different spin subband splitting, J_{sd} , and barrier height h_{B} .

observe a strong dependence of the total IEC, H^{ex} , on ε the MTJ should be made of materials with large I^{ex} contribution, larger than two other contributions. Figures 2 and 5 show that the Coulomb based exchange interaction is the largest contribution for strong spin subband splitting ($J_{\text{sd}} > U + E_{\text{F}}$) and not too small barrier height. Figure 7 shows the total exchange as a function of the dielectric constant at different J_{sd} and h_{B} . These curves can be fitted using the expression

$$H^{\text{ex}} = H_0^{\text{ex}} + \frac{I_1^{\text{ex}}}{\varepsilon}, \quad (32)$$

where $H_0^{\text{ex}} = H_{\text{h}}^{\text{ex}} + L^{\text{ex}}$ is the part of the total exchange coupling which does not depend on the dielectric permittivity and I_1^{ex} is the Coulomb based exchange coupling inside the insulator for $\varepsilon = 1$. Depending on the barrier height h_{B} , the thickness d of the insulator, and the spin subband splitting, the contribution H_0^{ex} can be either positive (green and black curves in figure 7) or negative (red and brown curves in figure 7). For negative H_0^{ex} the total IEC may change its sign with increasing the dielectric permittivity of the insulating layer (see the red curve). For small ε the IEC is positive (FM) while for large ε it is negative (AFM). The dependence of H^{ex} on ε can be used to distinguish this contribution from the hopping based exchange coupling. In experiment one can use an insulator with dielectric constant depending on some external parameter. In FE the dielectric permittivity depends on temperature and electric field. However, most FEs have rather large dielectric constants, $\varepsilon > 100$. These values of ε can suppress the Coulomb based exchange coupling. It is important to use FE with low dielectric permittivity such as TTF-CA [38, 39] or $\text{Hf}_{0.5}\text{Zr}_{0.5}\text{O}_2$ [40].

Figure 8 shows the temperature dependence of IEC, H^{ex} , with TTF-CA FE as an insulating layer. The FE Curie point of TTF-CA is $T_{\text{C}} = 56$ K [41, 42]. Using data of [41, 42] we find the temperature dependence of TTF-CA dielectric constant.

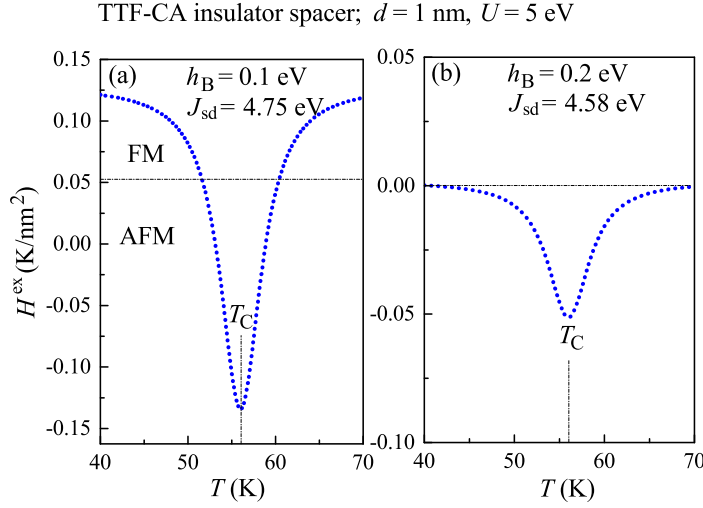


Figure 8. (Color online) Total IEC, H^{ex} in (28) as a function of temperature for MTJ with TTF-CA FE layer (ε is given by (33)). The system parameters are: $U = 5$ eV $d = 1$ nm, and (a) $J_{\text{sd}} = 4.75$ eV, $h_{\text{B}} = 0.1$ eV; (b) $J_{\text{sd}} = 4.58$ eV, $h_{\text{B}} = 0.2$ eV. T_{C} is the Curie point of TTF-CA ferroelectric.

Experimental data are fitted well with the following dependence of dielectric constant on temperature

$$\varepsilon(T) = 10 + \frac{25}{1 + (T - T_{\text{C}})^2/\Delta T^2}, \quad (33)$$

where $T_{\text{C}} = 56$ K is the Curie temperature of the ferroelectric-paraelectric (FE/PE) phase transition of TTF-CA and $\Delta T = 1.5$ K is the width of the peak. In the vicinity of the FE phase transition the dielectric permittivity of TTF-CA increases leading to decrease of the IEC. Panel (a) shows the change of sign of IEC from FM to AFM state in the vicinity of the FE/PE phase transition. Panel (b) shows the case of zero IEC away from the FE Curie point and finite IEC in the vicinity of T_{C} .

Figure 9 shows the interlayer exchange coupling, H^{ex} vs external electric field for $\text{Hf}_{0.5}\text{Zr}_{0.5}\text{O}_2$ FE layer. Here the voltage is applied across the MTJ with 1 nm $\text{Hf}_{0.5}\text{Zr}_{0.5}\text{O}_2$ insulating layer. This voltage produces an electric field inside the FE. We use data of [40] for the dependence of dielectric constant on the electric field for $\text{Hf}_{0.5}\text{Zr}_{0.5}\text{O}_2$ FE. The curves in figure 9 are shown at room temperature where $\text{Hf}_{0.5}\text{Zr}_{0.5}\text{O}_2$ is in the FE phase. The dielectric permittivity ε vs electric field has two branches due to hysteresis and it has two peaks in the vicinity of the switching fields, $E = \pm E_{\text{S}}$. These two peaks correspond to two dips in the H^{ex} curves. Panel (a) shows the change of sign of IEC with applied voltage: at zero voltage the coupling is AFM while at larger voltages the crossover from AFM to FM coupling occurs. Panel (b) shows the case of zero IEC at zero electric field and finite IEC at finite electric field. Thus, this panel explicitly shows the possible to control the IEC in MTJ using electric field.

Note that the applied voltage in FE MTJ changes not only the dielectric constant of the barrier but also the potential barrier itself and changes the FE polarization. These

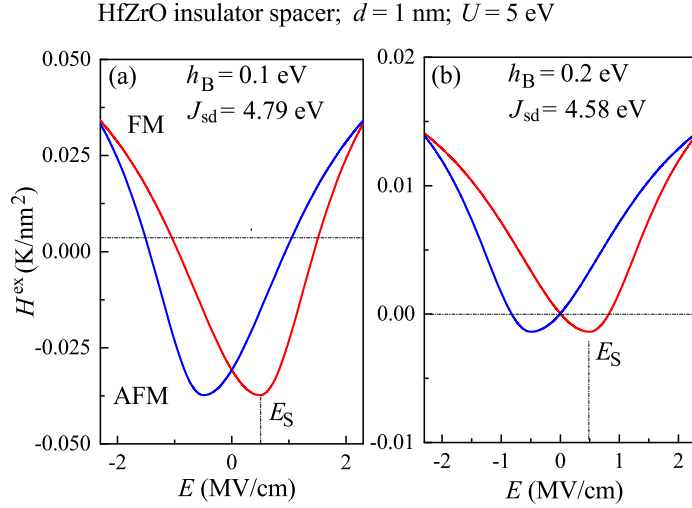


Figure 9. (Color online) Total IEC H^{ex} , (28) as a function of electric field inside of the insulating layer (voltage applied across MTJ) for MTJ with $\text{Hf}_{0.5}\text{Zr}_{0.5}\text{O}_2$ FE layer. The system parameters are: $U = 5$ eV $d = 1$ nm, and (a) $J_{\text{sd}} = 4.79$, eV $h_B = 0.1$ eV; (b) $J_{\text{sd}} = 4.58$, $h_B = 0.2$ eV. E_S is the FE polarization switching field.

effects are not taken into account in our consideration but they lead to the ME effect as well [30, 31, 32, 33, 10]. The ME effect in the above cited work is related to the hopping based IEC effect. The IEC effect in MTJ without FE barrier is quadratic in voltage in symmetric junctions [30, 31, 32, 33]. This is in contrast to the ME effect considered in the current manuscript having linear contribution at small voltages. From symmetry point of view, the polarization of the FE barrier should lead to the occurrence of linear contribution to the ME effect related to the hopping based IEC in symmetric MTJ. This case, however, was not considered in the literature. In asymmetric MTJ (considered in [10]) only the case of zero voltage was discussed. Due to MTJ asymmetry the polarization switching leads to variation of IEC even at zero voltage. A full comparison of ME effect due to the Coulomb based IEC and the hopping based IEC is beyond the scope of the current manuscript.

The dependence of the IEC on dielectric permittivity is due to coupling between magnetic and electric degrees of freedom in MTJ. This magneto-electric coupling has the Coulomb nature and allows controlling the magnetic state of MTJ. A similar effect was predicted semi-phenomenologically for granular magnets [43, 44, 45, 46].

7. Validity of our model

Below we discuss several assumptions and approximations of our theory.

1) We assume that the leads are “perfect” metals meaning that they screen the electric field completely. We use this assumption to calculate the electric field inside the insulating layer. We assume that the field created by charges is zero inside the metal. Similarly we assume that the Coulomb interaction inside the metal is a short-

range and is described by the δ -function. In fact, the electric potential created by a point charge located in a metal decays exponentially with distance, $\sim e^{-r/\lambda_{\text{TF}}}/r$, where λ_{TF} is Thomas-Fermi length. The electric field created by a charge located outside the metal also penetrates into the metal up to the distance λ_{TF} . Therefore in the vicinity of the metal surface (for distances less than λ_{TF}) our consideration is not valid. However, the Thomas-Fermi length is of the order of 0.05 nm and is much smaller than the characteristic decay length κ_0 of electron wave function and the thickness d of the insulating layer.

Also the metal-insulator barrier is not a step function as we assumed. The smearing of the boundary is comparable with λ_{TF} . In this region the classical description of screening inside the insulating barrier is not valid. We use the method of image charges to calculate screening. This approach works well if the distance from the metal surface is larger than the size of the exchange-correlation hole which is less than 0.1 nm. For distances less than 0.1 nm to the metal surface a quantum theory is required to describe the screening effects. Thus, our theory is not valid for MTJ with mono-layer insulating barrier [22].

2) In section 6 we discuss the ME coupling in MTJ due to the Coulomb based exchange interaction. To observe this coupling the FE layer should be present between magnetic leads. For strong exchange coupling the thickness of the insulating barrier should be about 1 nm. It is known that the FE Curie temperature decreases with decreasing the FE thickness [47, 48]. Some FEs show the critical thickness where FE properties can disappear. However, there are FEs that can keep their properties down to a single atomic layer thickness [47, 48]. In this paper we have not discussed the influence of size effects on the FE properties of insulating layer.

3) The voltage across the MTJ, necessary for creation of electric field in the insulating barrier, causes the electric and spin currents through the barrier. Such a current produces a spin transfer torque leading to the magnetic interaction between FM leads. This effect was not discussed here.

4) *Ab initio* calculations based on density functional theory mostly use the local spin density (LSD) approximation treating the indirect Coulomb interaction (exchange) as the short-range interaction, $\hat{H}_C \sim \delta(\mathbf{r}_1 - \mathbf{r}_2)$. This approach is valid only if the characteristic scales of the electron density variations are much larger than the screening radius and the Fermi length [49, 50]. Such an approximation works well inside the FM leads. However, inside the insulating layer the electron densities are low and the screening length exceeds the layer thickness. One can expect that the size of the exchange-correlation hole essentially exceeds the thickness of the insulating layer. In this case the Coulomb interaction is not the short range interaction any more. In this paper we take into account the long-range nature of the Coulomb interaction inside the insulating layer. Therefore, the LSD approximation can not be used to describe effects discussed in this paper.

5) The tunnelling matrix elements responsible for spin currents and the hopping based IEC also depend on the dielectric properties of the insulating matrix. In our

model we assume that potential profiles for electrons $U_{1,2}$ are the step functions. In reality the shape of potentials is affected by the dielectric constant of the insulating layer (see [51]). This effect requires a separate consideration.

8. Conclusion

We studied the exchange coupling in MTJ consisting of two FM layers separated by the insulating layer. We calculated the exchange coupling due to many-body effects (the inter-electron Coulomb interaction). The basic idea behind this mechanism is related to the fact that the wave functions of electrons located at different FM leads are overlapped inside the insulating layer. In combination with weak screening of electric field inside the insulator these electrons experience the indirect Coulomb interaction leading to interlayer magnetic coupling. We showed that the Coulomb based IEC can exceed the hopping based exchange contribution and found that these two mechanisms have essentially different dependence on system parameters.

We found that, in contrast to hopping based exchange, the Coulomb based exchange interaction is inversely proportional to the dielectric constant ε of the insulating layer. The dependence of the IEC on the dielectric properties of the insulating layer in MTJ is similar to ME effect where electric and magnetic degrees of freedom are coupled.

We calculated the IEC as a function of temperature and electric field (or voltage across the MTJ) for MTJ with insulating layer made of TTF-CA and $\text{Hf}_{0.5}\text{Zr}_{0.5}\text{O}_2$. We showed that in the vicinity of the FE phase transition of TTF-CA the IEC experiences large variations. We found that even the FM-AFM transition may occur in MTJ for some system parameters.

We found that IEC as a function of electric field (or applied voltage) shows strong variations. The electric field can cause the transition from AFM to FM coupling: for zero field the coupling is AFM while for finite field it is FM. This effect demonstrates the ME coupling in MTJ.

Acknowledgments

This research was supported by NSF under Cooperative Agreement Award EEC-1160504, the U.S. Civilian Research and Development Foundation (CRDF Global) and NSF PREM Award. O.U. was supported by Russian Science Foundation (Grant 16-12-10340).

Appendix A. Contribution of tunnelling to the Coulomb based IEC

The zero order wave function for FM configuration (the AFM wave function can be considered in a similar way) is given by the following Slater determinant

$$\Psi_0 = \frac{1}{\sqrt{N}} \begin{pmatrix} \psi_1^{s_1}(\mathbf{r}_1) & \dots & \psi_1^{s_1}(\mathbf{r}_{2n_0}) \\ \vdots & \ddots & \vdots \\ \phi_1^{s_{n_0+1}}(\mathbf{r}_1) & \dots & \phi_1^{s_{n_0+1}}(\mathbf{r}_{2n_0}) \\ \vdots & \ddots & \vdots \end{pmatrix}. \quad (\text{A.1})$$

States ψ_i and ϕ_j are chosen such that all the energy levels below E_F are filled: n_0 states in the left lead and n_0 states in the right lead. N is the normalization factor. Further we introduce the excited states as follows

$$\begin{aligned} \Psi_{ij}^s &= \\ &= \hat{b}_i^{s+} \hat{a}_j^s \Psi_0 = \frac{1}{\sqrt{N_{ij}}} \begin{pmatrix} \psi_1^{s_1}(\mathbf{r}_1) & \dots & \psi^{s_1}(\mathbf{r}_{2n_0}) \\ \vdots & \ddots & \vdots \\ \phi_{j-1}^{s_{n_0+j-1}}(\mathbf{r}_1) & \dots & \phi_{j-1}^{s_{n_0+j-1}}(\mathbf{r}_{2n_0}) \\ \psi_i^s(\mathbf{r}_1) & \dots & \psi_i^s(\mathbf{r}_{2n_0}) \\ \phi_{j+1}^{s_{n_0+j+1}}(\mathbf{r}_1) & \dots & \phi_{j+1}^{s_{n_0+j+1}}(\mathbf{r}_{2n_0}) \\ \vdots & \ddots & \vdots \end{pmatrix}. \end{aligned} \quad (\text{A.2})$$

The annihilation operator removes a line in the Slater determinant while the creation operator adds a line. N_{ij} is the normalization factor. We introduce the excited wave function as $\tilde{\Psi}_{ij}^s = \hat{a}_i^{s+} \hat{b}_j^s \Psi_0$. These wave functions correspond to single excitations with only one electron transferred between leads. Using the above excited states we can write the perturbed wave function as follows (see [37])

$$\Psi = (1 + \alpha_0) \Psi_0 + \sum_{s, i \notin S_0^s, j \in S_0^s} \beta_{ij}^s \Psi_{ij}^s + \sum_{s, i \notin S_0^s, j \in S_0^s} \tilde{\beta}_{ij}^s \tilde{\Psi}_{ij}^s, \quad (\text{A.3})$$

with

$$\beta_{ij}^s = \tilde{\beta}_{ij}^s = -\frac{T_{ij}^s}{\epsilon_i^s - \epsilon_j^s + \epsilon_c}, \quad (\text{A.4})$$

$$\alpha_0 = - \sum_{s, i \notin S_0^s, j \in S_0^s} \frac{|T_{ij}^s|^2}{(\epsilon_i^s - \epsilon_j^s + \epsilon_c)^2}, \quad (\text{A.5})$$

where T_{ij}^s is the tunnelling matrix element, ϵ_c is the charging energy, S_0 is the set of states in a single lead below the Fermi energy. The charging energy tends to zero for infinite leads, but it should still exceed the mean level spacing Δ ($\epsilon_c \sim 1/\Omega^{1/3}$, $\Delta \sim 1/\Omega$). Note that excited states with two or more electrons transferred from one lead to another are also possible. These states can be considered in a similar way. The Coulomb contribution to the energy of FM configuration is given by

$$\begin{aligned} H_C^{\text{FM}} &= \langle \Psi | \hat{H}_C | \Psi \rangle = \\ &= (1 + 2\alpha_0) \langle \Psi_0 | \hat{H}_C | \Psi_0 \rangle + 2 \sum_{ij} |\beta_{ij}^s|^2 \langle \Psi_{ij} | \hat{H}_C | \Psi_{ij} \rangle + \dots \end{aligned} \quad (\text{A.6})$$

In our manuscript we change it with the expression $\langle \Psi_0 | \hat{H}_C | \Psi_0 \rangle$. The terms of the type $\langle \Psi_0 | \hat{H}_C | \Psi_{ij} \rangle$ not written in (A.6) correspond to tunnelling of electrons between the leads due to the Hamiltonian \hat{H}_C . These terms in fact are taken into account in tunnelling matrix elements T_{ij}^s . The potential profile for s-electrons, $\hat{U}_{1,2}$ appears due to the mean electrostatic potential created by ions and s-electrons themselves. Also, we neglect the electron-electron scattering within leads, $\langle \Psi_{lk} | \hat{H}_C | \Psi_{ij} \rangle$ ($k \neq i, j, l \neq i, j$).

The coefficients $\beta_{ij}^s \sim e^{-\kappa d}$ are small. Therefore, in the last term of (A.6) we can calculate $\langle \Psi_{ij} | \hat{H}_C | \Psi_{ij} \rangle$ considering leads as independent (non-interacting). The state Ψ_{ij} is different from the state Ψ_0 by adding one electron into one lead and removing of one electron from another lead. The Coulomb energy of a metallic lead is given by the expression [36]

$$U_C^L = \epsilon_c n^2 + \frac{\Delta}{\pi} (S - S_0)^2, \quad (\text{A.7})$$

where n is the excessive charge and $S - S_0$ is the excessive spin (deviation of the total spin from its equilibrium value). The non-zero equilibrium spin, S_0 appears in our consideration due to the interaction with d-electrons. Taking (A.7) into account we can write

$$\langle \Psi_{ij} | \hat{H}_C | \Psi_{ij} \rangle \approx \langle \Psi_0 | \hat{H}_C | \Psi_0 \rangle + \epsilon_c + O(\Delta). \quad (\text{A.8})$$

Substituting (A.5) and (A.8) into (A.6) we get

$$H_C^{\text{ex}} = \langle \Psi_0 | \hat{H}_C | \Psi_0 \rangle + 4\epsilon_c \sum_{ij} |\beta_{ij}^s|^2 + \dots \quad (\text{A.9})$$

The hopping based contribution can be written using the same language in the form

$$H_0^{\text{FM}} = \dots + \sum_{ij} |\beta_{ij}^s|^2 \langle \Psi_{ij} | \hat{H}_0 | \Psi_{ij} \rangle, \quad (\text{A.10})$$

where

$$\langle \Psi_{ij} | \hat{H}_0 | \Psi_{ij} \rangle = \epsilon_i^s - \epsilon_j^s + \langle \Psi_0 | \hat{H}_0 | \Psi_0 \rangle. \quad (\text{A.11})$$

Where $\epsilon_i - \epsilon_j$ is the difference of kinetic energies in states i and j . This term describes virtual transitions of electrons from state i (under the Fermi surface) in one lead to state j (above the Fermi level) in another lead. Effective energy region in the vicinity of the Fermi level contributing to the hopping based exchange interaction can be estimated as follows $\hbar^2 \kappa_0 / d \approx 100$ K (see [8]). We can estimate $\epsilon_i - \epsilon_j \sim \hbar^2 \kappa_0 / d \approx 100$ K. Using this estimation we have

$$H_0^{\text{FM}} = \dots + \frac{\hbar^2 \kappa_0}{d} \sum_{ij} |\beta_{ij}^s|^2. \quad (\text{A.12})$$

Obviously, $\hbar^2 \kappa_0 / d \gg \epsilon_c$. Comparing (A.12) and (A.9) one can see that the last term in (A.9) can be neglected in comparison to the hopping based contribution.

Note that the summation in the matrix element $\langle \Psi_0 | \hat{H}_C | \Psi_0 \rangle$ is over all pair of electrons since the Coulomb matrix element does not depend on the perpendicular momentum. The matrix element β_{ij}^s is non-zero only for transitions with conservation

of perpendicular momentum \mathbf{k}_\perp . Therefore, summation in the last term of (A.9) is over pairs of states with the same \mathbf{k}_\perp . Therefore, there are much less pairs participating in the last term of (A.9) in comparison to the number of state pairs contributing to the first term of (A.9), and $\langle \Psi_0 | \hat{H}_C | \Psi_0 \rangle \gg \epsilon_c \sum_{ij} |\beta_{ij}^s|^2$. Thus, we can neglect the last term in (A.9) and calculate the Coulomb based IEC averaging over the unperturbed function Ψ_0 .

Appendix B. Contribution to the IEC from the insulating layer

Here we calculate the following integral

$$\begin{aligned} \tilde{I}_{\text{ex}}^- &= \frac{-\Omega^2}{(2\pi)^6 S} \int d^3 r_1 d^3 r_2 d^3 k_1 d^3 k_2 \hat{U}_C^I(\mathbf{r}_1, \mathbf{r}_2) \times \\ &\times \tilde{\rho}(z_1) (\tilde{\rho}(z_2))^* e^{i(\mathbf{k}_{1\perp} - \mathbf{k}_{2\perp}) \cdot \mathbf{r}_{1\perp}} e^{-i(\mathbf{k}_{1\perp} - \mathbf{k}_{2\perp}) \cdot \mathbf{r}_{2\perp}} + . \end{aligned} \quad (\text{B.1})$$

The integration over the coordinates \mathbf{r}_1 and \mathbf{r}_2 in (B.1) is performed over the region between the leads. Renaming variables $\mathbf{k}_{1\perp} \rightarrow \mathbf{k}_{2\perp}$ and $\mathbf{k}_{2\perp} \rightarrow \mathbf{k}_{1\perp}$ makes the integrand complex conjugate, however the whole integral stays the same meaning that only the real part of the integral is finite. Below we consider the real part of the integrand

$$\begin{aligned} \tilde{I}_{\text{ex}}^- &= \frac{-\Omega^2}{(2\pi)^6 S} \int d^3 r_1 d^3 r_2 d^3 k_1 d^3 k_3 \times \\ &\times \tilde{\rho}(z_1) \hat{U}_C^I(\mathbf{r}_1, \mathbf{r}_2) (\tilde{\rho}(z_2))^* \times \\ &\{ \cos((\mathbf{k}_{1\perp} - \mathbf{k}_{2\perp}) \cdot \mathbf{r}_1) \cos((\mathbf{k}_{1\perp} - \mathbf{k}_{2\perp}) \cdot \mathbf{r}_2) + \\ &+ \sin((\mathbf{k}_{1\perp} - \mathbf{k}_{2\perp}) \cdot \mathbf{r}_1) \sin((\mathbf{k}_{1\perp} - \mathbf{k}_{2\perp}) \cdot \mathbf{r}_2) \}. \end{aligned} \quad (\text{B.2})$$

Both terms (with $\sin()$ and $\cos()$) give the same contribution. Thus, we consider one term with numerical factor 2

$$\begin{aligned} \tilde{I}_{\text{ex}}^- &= \frac{-2\Omega^2}{(2\pi)^6 S} \int d^3 r_1 d^3 r_2 d^3 k_1 d^3 k_2 \times \\ &\times \tilde{\rho}(z_1) \hat{U}_C^I(\mathbf{r}_1, \mathbf{r}_2) (\tilde{\rho}(z_2))^* \times \\ &\times \cos((\mathbf{k}_{1\perp} - \mathbf{k}_{2\perp}) \cdot \mathbf{r}_1) \cos((\mathbf{k}_{1\perp} - \mathbf{k}_{2\perp}) \cdot \mathbf{r}_2). \end{aligned} \quad (\text{B.3})$$

The last integral can be written in the form

$$\begin{aligned} \tilde{I}_{\text{ex}}^- &= \frac{-4\Omega^2}{(2\pi)^6 S} \int_0^{k_F^-} dk_{1z} \int_0^{k_{1z}} dk_{2z} \int d^3 r_1 d^3 r_2 \times \\ &\times \int_{|\mathbf{k}_{1\perp}|^2 < (k_F^-)^2 - k_{1z}^2} d^2 k_{1\perp} \int_{|\mathbf{k}_{2\perp}|^2 < (k_F^-)^2 - k_{2z}^2} d^2 k_{2\perp} \tilde{\rho}(z_1) (\tilde{\rho}(z_2))^* \times \\ &\times \hat{U}_C^I(\mathbf{r}_1, \mathbf{r}_2) \cos((\mathbf{k}_{1\perp} - \mathbf{k}_{2\perp}) \cdot \mathbf{r}_1) \cos((\mathbf{k}_{1\perp} - \mathbf{k}_{2\perp}) \cdot \mathbf{r}_2). \end{aligned} \quad (\text{B.4})$$

Equation (B.4) shows that the exchange interaction is the sum of matrix elements of the Coulomb interaction between the effective charges. These charges decay toward the middle of the barrier, $z = 0$, and oscillate in the (x, y) -plane. The oscillations are coherent and have the same phase.

The normalized matrix element of the effective Coulomb interaction is given by the expression

$$W_I = \frac{1}{S} \int d^3r_1 d^3r_2 \tilde{\rho}(z_1) (\tilde{\rho}(z_2))^* \times \hat{U}_C^I(\mathbf{r}_1, \mathbf{r}_2) \cos((\mathbf{k}_{1\perp} - \mathbf{k}_{2\perp})\mathbf{r}_1) \cos((\mathbf{k}_{1\perp} - \mathbf{k}_{2\perp})\mathbf{r}_2). \quad (\text{B.5})$$

We introduce the notations $\rho_0^2 = |e\tau_i^{s*}\tau_j^{s'}|/\Omega|^2$, $\Delta\kappa = \kappa_1 - \kappa_2$, $\mathbf{q} = \mathbf{k}_{1\perp} - \mathbf{k}_{2\perp}$ ($q = |\mathbf{q}|$). To evaluate the matrix element we calculate the electric field created by the effective charges. Due to periodic harmonic variations of the electric charge the field has the same harmonic variations. The electric field inside the metallic leads is zero since it is screened by the surface charges which vary with the wave vector \mathbf{q} .

Consider the z-component of the electric field at $\mathbf{r}_\perp = 0$. At this symmetry point the field has no (x,y)-plane components. The field created by the charge in the gap has the form

$$\begin{aligned} E_z^{\text{ch}}(z) &= \frac{\rho_0}{4\pi\epsilon_0\epsilon} \int_0^{2\pi} d\varphi \int_0^\infty r_\perp dr_\perp \int_{-d/2}^{d/2} d\tilde{z} \times \\ &\times \frac{\cos(qr_\perp \cos(\varphi))(z - \tilde{z})e^{-\Delta\kappa\tilde{z}}}{(r_\perp^2 + (z - \tilde{z})^2)^{3/2}} = \\ &= \frac{\rho_0}{2\epsilon_0\epsilon} \left\{ \frac{e^{-qz}}{q - \Delta\kappa} (e^{(q-\Delta\kappa)z} - e^{-(q-\Delta\kappa)d/2}) + \right. \\ &\left. + \frac{e^{qz}}{q + \Delta\kappa} (e^{-(q+\Delta\kappa)d/2} - e^{-(q+\Delta\kappa)z}) \right\}. \end{aligned} \quad (\text{B.6})$$

The electric field created by the surface metal charges is given by the expression

$$E_z^{\text{m}}(z) = \frac{\rho_0}{2\epsilon_0\epsilon} (\sigma_2 e^{-q(z+d/2)} + \sigma_1 e^{q(z-d/2)}), \quad (\text{B.7})$$

where the surface charges $\sigma_{1,2}$ are

$$\sigma_{1(2)} = \frac{\sigma_{1(2)}^0 e^{qd} + \sigma_{2(1)}^0}{e^{qd} - e^{-qd}}, \quad (\text{B.8})$$

with

$$\begin{aligned} \sigma_1^0 &= \frac{e^{-qd/2}}{q - \Delta\kappa} (e^{(q-\Delta\kappa)d/2} - e^{-(q-\Delta\kappa)d/2}), \\ \sigma_2^0 &= \frac{e^{-qd/2}}{q + \Delta\kappa} (e^{-(q+\Delta\kappa)d/2} - e^{(q+\Delta\kappa)d/2}). \end{aligned} \quad (\text{B.9})$$

The total value of the z-component of electric field due to the charge $\rho^{(1)}$ is the sum, $E_z^{(1)} = E_z^{\text{ch}} + E_z^{\text{m}}$. Similarly we can calculate the amplitude of the in-plane field component $E_x^{(1)}$. Its spatial variation is shifted by a half period $1/(2q)$.

Both charges in (B.4) have the same period of oscillations and the same phase. The field produced by the charge $\rho^{(2)}$ is the same as the field $\mathbf{E}^{(1)}$, ($E_z^{(2)}(z) = E_z^{(1)}(z)$), ($E_x^{(2)}(z) = E_x^{(1)}(z)$). The surface density (density per surface area of leads) of interaction energy can be calculated as follows $W_I = (\epsilon_0\epsilon/2)(\int dz E_z^{(1)}(z) E_z^{(1)}(z) +$

$\int dz E_x^{(1)}(z) E_x^{(1)}(z)$, where integration goes over the region $|z| < d/2$. Finally, the matrix element can be estimated as follows

$$W_I = W_{Ix} + W_{Iz}, \quad (\text{B.10})$$

where

$$\begin{aligned} W_{Iz} &= \frac{\rho_0^2}{8\varepsilon_0\varepsilon} \left\{ (\alpha_1^2 + \alpha_2^2) \frac{\sinh(dq)}{q} + \alpha_3^2 \frac{\sinh(d\Delta\kappa)}{q} \right. \\ &\quad + 2\alpha_1\alpha_2d + 4\alpha_1\alpha_3 \frac{\sinh((\Delta\kappa + q)d/2)}{\Delta\kappa + q} \\ &\quad \left. + 4\alpha_2\alpha_3 \frac{\sinh((\Delta\kappa - q)d/2)}{\Delta\kappa - q} \right\}, \\ W_{Ix} &= \frac{\rho_0^2}{8\varepsilon_0\varepsilon} \left\{ (\tilde{\alpha}_1^2 + \tilde{\alpha}_2^2) \frac{\sinh(dq)}{q} + \tilde{\alpha}_3^2 \frac{\sinh(d\Delta\kappa)}{q} \right. \\ &\quad + 2\tilde{\alpha}_1\tilde{\alpha}_2d + 4\tilde{\alpha}_1\tilde{\alpha}_3 \frac{\sinh((\Delta\kappa + q)d/2)}{\Delta\kappa + q} \\ &\quad \left. + 4\tilde{\alpha}_2\tilde{\alpha}_3 \frac{\sinh((\Delta\kappa - q)d/2)}{\Delta\kappa - q} \right\}, \end{aligned} \quad (\text{B.11})$$

with

$$\alpha_1 = e^{-qd/2} \sigma_2 - \frac{e^{-(q-\Delta\kappa)d/2}}{q - \Delta\kappa}, \quad (\text{B.12})$$

$$\tilde{\alpha}_1 = -e^{-qd/2} \sigma_2 - \frac{e^{-(q-\Delta\kappa)d/2}}{q - \Delta\kappa}, \quad (\text{B.13})$$

$$\alpha_2 = e^{-qd/2} \sigma_1 + \frac{e^{-(q+\Delta\kappa)d/2}}{q + \Delta\kappa}, \quad (\text{B.14})$$

$$\tilde{\alpha}_2 = e^{-qd/2} \sigma_1 - \frac{e^{-(q+\Delta\kappa)d/2}}{q + \Delta\kappa}, \quad (\text{B.15})$$

$$\alpha_3 = \frac{2\Delta\kappa}{q^2 - \Delta\kappa^2}, \quad \tilde{\alpha}_3 = \frac{-2q}{q^2 - \Delta\kappa^2}. \quad (\text{B.16})$$

Introducing W_I into (B.4) we arrive to the final expression for \tilde{I}_{ex}^-

$$\begin{aligned} \tilde{I}_{\text{ex}}^- &= -\frac{e^2}{32\pi^4\varepsilon_0\varepsilon} \int_0^{k_F^-} \int_0^{k_1} dk_1 dk_2 |(\tau_1^-)^* \tau_2^-|^2 e^{-d(\kappa_1^- + \kappa_2^-)} \times \\ &\quad \times \int_0^{k_2^{\text{max}} + k_1^{\text{max}}} q \omega_I(q) dq \int_0^{(k_2^{\text{max}} + k_1^{\text{max}})/2} k \zeta(k, q) dk, \end{aligned} \quad (\text{B.17})$$

where

$$\omega_I(q) = \frac{8\varepsilon_0\varepsilon W_I(q)}{\rho_0^2}. \quad (\text{B.18})$$

We introduced the following functions

$$\zeta = \begin{cases} 0, & (\phi_2 < \phi_3) \text{ or } (\phi_1 < \phi_3), \\ \phi_1 - \phi_3, & \text{otherwise,} \end{cases} \quad (\text{B.19})$$

where

$$\phi_1(k, q) = \begin{cases} 0, & k > k_1^{\max} + q/2, \\ \frac{\pi + \pi \text{sign}(k_1^{\max} - q/2)}{2}, & k < |k_1^{\max} - q/2|, \\ \arccos\left(\frac{k^2 + q^2/4 - (k_1^{\max})^2}{qk}\right), & \text{otherwise.} \end{cases} \quad (\text{B.20})$$

$$\phi_2(k, q) = \begin{cases} \pi, & k < k_2^{\max} - q/2, \\ \arccos\left(\frac{k^2 + q^2/4 - (k_2^{\max})^2}{qk}\right), & \text{otherwise.} \end{cases} \quad (\text{B.21})$$

$$\phi_3(k, q) = \pi - \phi_2(k, q). \quad (\text{B.22})$$

In a similar way one can calculate the integrals \tilde{I}_{ex}^+ and \tilde{I}_{ex}^- .

References

- [1] A. D. Kent and D. C. Worledge. *Nature Nanotechnology*, 10:187, 2015.
- [2] Claude Chappert, Albert Fert, and Frederic Nguyen Van Dau. *Nature Materials*, 6:813, 2007.
- [3] W. H. Butler and A. Gupta. *Nature Materials*, 3:845, 2015.
- [4] Gary A. Prinz. *Science*, 282:1660, 1998.
- [5] Adrian Cho. *Science*, 296:246, 2002.
- [6] K. Ando, S. Fujita, J. Ito, S. Yuasa, Y. Suzuki, Y. Nakatani, T. Miyazaki, and H. Yoda. *J. Appl. Phys.*, 115:172607, 2014.
- [7] M. Julliere. *Phys. Lett.*, 54A:225, 1975.
- [8] J C Slonczewski. *Phys. Rev. B*, 39:6995, 1989.
- [9] P Bruno. *Phys. Rev. B*, 52:411, 1995.
- [10] M. Ye. Zhuravlev, E. Y. Tsymbal, and A. V. Vedyayev. *Phys. Rev. Lett.*, 94:026806, 2005.
- [11] J. M. Pruneda, R. Robles, S. Bouarab, J. Ferrer, and A. Vega. *Phys. Rev. B*, 65:024440, 2001.
- [12] T. Katayama, S. Yuasa, J. Velez, M. Ye. Zhuravlev, S. S. Jaswal, and E. Y. Tsymbal. *Appl. Phys. Lett.*, 89:112503, 2006.
- [13] Paul M. Haney, Christian Heiliger, and Mark D. Stiles. *Phys. Rev. B*, 79:054405, 2009.
- [14] J. P. Velez, M. Ye. Zhuravlev, K. D. Belashchenko, S. S. Jaswal, E. Y. Tsymbal, T. Katayama, and S. Yuasa. *IEEE Transactions on Magnetism*, 43:2770, 2007.
- [15] M Ye Zhuravlev, A V Vedyayev, and E Y Tsymbal. *J. Phys.: Condens. Matter*, 22:352203, 2010.
- [16] R. R. Gareev, D. E. Burgler, M. Buchmeier, R. Schreiber, and P. Grunberg. *Appl. Phys. Lett.*, 81:1264, 2002.
- [17] R. R. Gareev, L. L. Pohlmann, S. Stein, D. E. Burgler, and P. A. Grunberg and M. Siegel. *J. Appl. Phys.*, 93:8038, 2003.
- [18] J. Faure-Vincent, C. Tiusan, C. Bellouard, E. Popova, M. Hehn, F. Montaigne, and A. Schuhl. *Phys. Rev. Lett.*, 89:107206, 2002.
- [19] P. A. A. van der Heijden, P. J. H. Bloemen, J. M. Metselaar, R. M. Wolf, J. M. Gaines, J. T. W. M. van Eemeren, P. J. van der Zaag, and W. J. M. de Jonge. *Phys. Rev. B*, 55:11569, 1997.
- [20] H. Yanagihara, Yuta Toyoda, and Eiji Kita. *J. Appl. Phys.*, 101:09D101, 2007.
- [21] Witold Skowronski, Tomasz Stobiecki, Jerzy Wrona, Karsten Rott, Andy Thomas, Gunter Reiss, and Sebastiaan van Dijken. *J. Appl. Phys.*, 107:093917, 2010.
- [22] A. Koziol-Rachwal, T. Slezak, M. Slezak, K. Matlak, E. Mlynczak, N. Spiridis, and J. Korecki. *J. Appl. Phys.*, 115:104301, 2014.
- [23] C. H. Marrows, N. Wiser, B. J. Hickey, T. P. A. Hase, and B.K. Tanner. *J. Phys.: Condens. Mat.*, 11:81, 1999.
- [24] J. C. S. Kools. *J. Appl. Phys.*, 77:2993, 1999.
- [25] M. Zhuravlev, J. Velez, A. Vedyayev, and E. Tsymbal. *J. Magn. Magn. Mater.*, 300:277, 2006.

- [26] S V Vonsovskii. *Magnetism*. Wiley, New York, 1974.
- [27] L D Landau and E M Lifshitz. *Quantum Mechanics Nonrelativistic Theory, Course of Theoretical Physics*, volume 3. Nauka, Moscow, 3 edition, 1976.
- [28] W. Eerenstein, N. D. Mathur, and J. F. Scott. *Nature*, 442:759, 2006.
- [29] R. Ramesh and Nicola A. Spaldin. *Nature Mat.*, 6:21, 2007.
- [30] Jiang Xiao, Gerrit E. W. Bauer, and Arne Brataas. *Phys. Rev. B*, 77:224419, 2008.
- [31] Se-Chung Oh, Seung-Young Park, Aurlien Manchon, Mairbek Chshiev, Jae-Ho Han, Hyun-Woo Lee, Jang-Eun Lee, Kyung-Tae Nam, Younghun Jo, Yo-Chan Kong, Bernard Dieny, and Kyung-Jin Lee. *Nature Phys.*, 5:898, 2009.
- [32] Hitoshi Kubota, Akio Fukushima, Kay Yakushiji, Taro Nagahama, Shinji Yuasa, Koji Ando, Hiroki Maehara, Yoshinori Nagamine, Koji Tsunekawa, David D. Djayaprawira, Naoki Watanabe, and Yoshishige Suzuki. *Nature Phys.*, 4:37, 2008.
- [33] Jack C. Sankey, Yong-Tao Cui, Jonathan Z. Sun, John C. Slonczewski, Robert A. Buhrman, and Daniel C. Ralph. *Nature Phys.*, 4:67, 2008.
- [34] J. C. Slonczewski. *Phys. Rev. B*, 71:024411, 2005.
- [35] Ioannis Theodonis, Nicholas Kioussis, Alan Kalitsov, Mairbek Chshiev, and W. H. Butler. *Phys. Rev. Lett.*, 97:237205, 2006.
- [36] I. L. Aleiner, P. W. Brouwer, and L. I. Glazman. *Phys. Rep.*, 358:309, 2002.
- [37] O. G. Udalov and I. S. Beloborodov. *arXiv:1606.02622v1*, 2016.
- [38] H. Okamoto, T. Mitani, Y. Tokura, S. Koshihara, T. Komatsu, Y. Iwasa, T. Koda, and G. Saito. *Phys. Rev. B*, 43:8224, 1991.
- [39] K. Kobayashi, S. Horiuchi, R. Kumai, F. Kagawa, Y. Murakami, and Y. Tokura. *Phys. Rev. Lett.*, 108:237601, 2012.
- [40] Johannes Muller, Tim S. Boscke, Uwe Schroder, Stefan Mueller, Dennis Brauhaus, Ulrich Bottger, Lothar Frey, and Thomas Mikolajick. *Nano Letters*, 12:4318, 2012.
- [41] M Huth, A Rippert, R Sachser, and L Keller. *Mater. Res. Expr.*, 1:046303, 2014.
- [42] M Huth, F Kolb, and H Plank. *Appl. Phys. A*, 117:1689, 2014.
- [43] O G Udalov, N M Chtchelkatchev, and I S Beloborodov. *Phys. Rev. B*, 89:174203, 2014.
- [44] O G Udalov, N M Chtchelkatchev, and I S Beloborodov. *J. Phys.: Condens. Matter*, 27:186001, 2015.
- [45] O G Udalov, N M Chtchelkatchev, and I S Beloborodov. *Phys. Rev. B*, 92:045406, 2015.
- [46] A M Belemuk, O G Udalov, N M Chtchelkatchev, and I S Beloborodov. *J. Phys.: Condens. Matter*, 28:126001, 2016.
- [47] V. M. Fridkin. *Phys. Usp.*, 49:193, 2006.
- [48] V. M. Fridkin, R. V. Gaynutdinov, and S. Ducharme. *Phys. Usp.*, 53:199, 2010.
- [49] J. P. Perdew and A. Zunger. *Phys. Rev. B*, 23:5048, 1981.
- [50] O. Gunnarsson and B. I. Lundqvist. *Phys. Rev. B*, 13:4274, 1976.
- [51] E. Burstein and S. Lundqvist. *Tunneling Phenomena in Solids*. Plenum Press, New York, 1969.